Biomedical Engineering Advances 4 (2022) 100065

Contents lists available at ScienceDirect

Biomedical Engineering Advances

journal homepage: www.journals.elsevier.com/biomedical-engineering-advances

3D printed biomimetic flexible blood vessels with iPS cell-laden hierarchical multilayers

Sung Yun Hann [a], Haitao Cui [a], Guibin Chen [b], Manfred Boehm [b], Timothy Esworthy [a], Lijie Grace Zhang [a,c,d,e,*]

[a] Department of Mechanical and Aerospace Engineering, The George Washington University, Washington, D.C. 20052, USA
[b] Laboratory of Cardiovascular Regenerative Medicine, Translational Vascular Medicine Branch, National Heart, Lung, and Blood Institute, National Institutes of Health (NIH), Bethesda, MD 20892, USA
[c] Department of Electrical and Computer Engineering, The George Washington University, Washington, D.C. 20052, USA
[d] Department of Biomedical Engineering, The George Washington University, Washington, DC 20052, USA
[e] Department of Medicine, The George Washington University Medical Center, Washington, DC 20052, USA

ARTICLE INFO

Keywords:
3D printing
Artificial vessel
Flexible polymer
Induced pluripotent stem cell
Tissue engineering

ABSTRACT

Successful recovery from vascular diseases has typically relied on the surgical repair of damaged blood vessels (BVs), with the majority of current approaches involving the implantation of autologous BVs, which is plagued by donor site tissue damage. Researchers have attempted to develop artificial vessels as an alternative solution to traditional approaches to BV repair. However, the manufacturing of small-diameter (< 6 mm) BVs is still considered one of the biggest challenges due to its difficulty in the precise fabrication and the replication of biomimetic architectures. In this study, we successfully developed 3D printed flexible small-diameter BVs that consist of smooth muscle cells and a vascularized endothelium. In the developed artificial BV, a rubber-like elastomer was printed as the outermost layer of the vessel, which demonstrated enhanced mechanical properties, while and human induced pluripotent stem cell (iPSC)-derived vascular smooth muscle cells (iSMCs) and endothelial cells (iECs) embedded fibrinogen solutions were coaxially extruded with thrombin solution to form cell-laden fibrin gel inner layers. Our results showed that the 3D BVs possessed proper mechanical properties, and the cells in the fibrin layers substantially proliferated over time to form a stable BV construct. Our study demonstrated that the 3D printed flexible small-diameter BV using iPSCs could be a promising platform for the treatment of vascular diseases.

1. Introduction

The fundamental goal of biomedical engineering is the development of viable organs and tissues to repair the damaged human body. Regarding that, a considerable amount of research has been dedicated to regeneration of various tissues by many biomedical engineers during the past decades. While most previous studies focused on the regeneration of specific organs and tissues, research related to the blood vessel (BV) has been slow in progress. In the human body, vascular networks are critically significant as they perform the tasks to maintain the function of tissue and organs, such as oxygen and nutrition supply, and waste removal [1–3]. Being noted by the American Heart Association, BV diseases (cardiovascular, artery, and venous) account for the leading cause of mortality in the US in 2021 [4]. In other words, BV-related diseases, such as thrombosis and atherosclerosis as well as the repair of damaged BVs remain one of the biggest challenges [5,6]. Although autologous BVs have been known as the fundamental solution to that, the lack of donor autograft interferes with its availability as a clinical treatment [6,7]. Recently, artificial vessels have risen as a new candidate to remedy BV diseases [8–10], and some studies have reported meaningful results from *in vitro* to clinical implantation stages [1,11,12]. However, the fabrication of artificial BV with a small diameter (< 6 mm) is still considered one of the unsolved problems due to the complication of microfabrication. Additionally, the failure of small-diameter BV is typically caused by deficient patency due to the progress of atherosclerosis [5,13–17]. Thus, it is crucial to emphasize that the successful

* Corresponding author at: Department of Mechanical and Aerospace Engineering, The George Washington University, Science and Engineering Hall 3590, 800 22nd Street NW, Washington DC 20052.
E-mail address: lgzhang@email.gwu.edu (L.G. Zhang).

https://doi.org/10.1016/j.bea.2022.100065
Received 15 September 2022; Received in revised form 21 November 2022; Accepted 26 November 2022
Available online 28 November 2022

formation of small-diameter artificial BVs is the most significant key to develop and recover damaged circulatory systems in the human body.

To embody these properties of small-diameter BVs, three-dimensional (3D) printing techniques, such as fused deposition modeling (FDM), stereolithography (SLA), digital light processing (DLP), inkjet printing, extrusion-based printing, and others, have been widely utilized to fabricate artificial vessels, based on their remarkable reproducibility, controllability, and repeatability [1,2,18]. Among the listed 3D printing systems, extrusion-based printing is a decent candidate for the quick fabrication of artificial BV constructs. Traditionally, conventionally available bioplastic filaments, including polycaprolactone (PCL) or polylactic acid (PLA), have been utilized to engineer BV, and several corresponding studies have reported noticeable results [19–23]. However, the notorious issues with the use of these materials include (1) the lack of innate flexibility compared to the natural BV, and (2) the insufficient capacity to support cell growth for BV regeneration.

To overcome these obstacles, synthetic biopolymers that have sufficient flexibility and biocompatibility were considered as a suitable alternative. However, the fabrication of BV with synthetic biopolymers possibly yields a lack of biocompatibility, which would result in insufficient cell adhesion and proliferation. Previous studies have used collagen or fibrinogen-based natural biomaterials to provide ideal biocompatibility, excellent cell adhesion, and proliferation environment for the regeneration of BV and other tissues [24–27]. However, the severe drawback of these natural biomaterials is their poor mechanical properties that fail to endure internal or external stresses. Therefore, integrating the benefits of synthetic and natural materials can be an ideal candidate to resolve challenges in the current artificial BV fabrication studies. To carry out the task, we propose to use a rubber-like elastomer called GEL-LAY PORO-LAY (Gel-Lay) to enhance flexibility and fibrin to promote biocompatibility with the combination of FDM 3D printing and cell-laden coaxial bioplotting as an additive manufacturing tool. Moreover, we used human induced pluripotent stem cell-derived vascular smooth muscle cells (iSMCs) and human induced pluripotent stem cell-derived endothelial cells (iECs) to regenerate the smooth muscle and endothelium of BV due to their advantages in many aspects. Generally, it has been widely known that human induced pluripotent stem cell (iPSC)-based technology is beneficial in biomedical applications due to its minimal immune response, unlimited cell resource, and ethical issue-free privilege [28,29]. Specifically, iSMCs are a great candidate to replace human vascular smooth muscle cells (VSMCs) for a BV study as the main drawbacks of VSMCs are relatively low proliferation capability and potential culture senescence [30,31]. In addition, the development of iECs contributed to overcoming the deficit of autologous endothelial cells (ECs) by providing a large number of patient-specific cells and healing BV diseases [32].

Having this anatomical, technical, and material background in mind, the fabrication of a 3D printed architecture with organized integration of the aforementioned characteristics could be motivated. In this pilot study, an extensively flexible and biomimetic BV implant with the mix of a natural biomaterial and a synthetic polymer is novelly demonstrated, which can remedy weaknesses of current research due to poor stretchability of the protection layer (conventional natural materials) and concerns associated with the biocompatibility of inner layers in the related field. The fabricated biomimetic BV consists of three layers: (1) an outmost (supporting/protection) layer with Gel-Lay, which is majorly comprised of polyamide as a functional component and polyvinyl alcohol (PVA) as a soluble binder and conventionally obtainable at a low-cost [33], (2) a middle layer of fibrin gel having iSMCs embedded, and (3) an innermost layer with iECs in the fibrin gel. Based on these, the main goal of this study is to develop multilayer BVs possessing previously mentioned biomimetic and physical characteristics via 3D printing techniques *in vitro* as shown in Fig.1. Along with the proliferation quantification of iSMCs and iECs over time intervals, the suitability of our BVs for other cells including human coronary artery smooth muscle

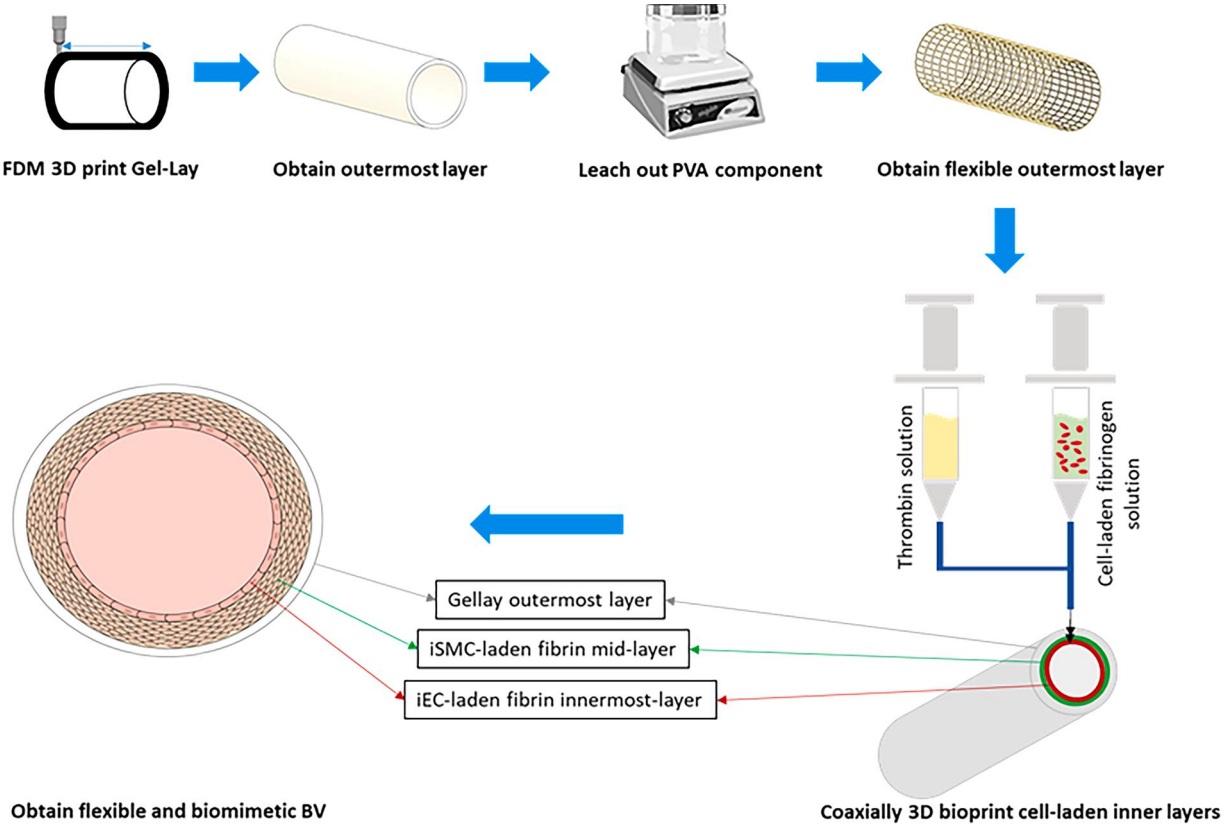

Fig. 1. A schematic illustration of the overall experimental design.

cells (hSMCs) and human umbilical vein endothelial cells (HUVECs) was also tested. Furthermore, the specific markers of iSMCs, anti-alpha-smooth muscle actin (α-SMA) and iECs, anti-cluster of differentiation 31 (CD31) were used to evaluate the bioactivity of the cells, and CellTracker™ staining was performed to observe the distribution and growth of both cells simultaneously.

2. Materials and methods

The reagents and solvents and reagents used in this study were purchased from Sigma-Aldrich unless otherwise specified.

2.1. Preparation and fabrication of 3D blood vessels

Gel-Lay filament (MatterHackers, Lake Forest, CA) that consists of polyamide (functional component) and PVA (soluble binder) [33–35] as an outermost material was printed by an FDM 3D printer (MakerBot) under the following conditions: 215 °C (nozzle temperature), 800 μm (nozzle diameter), and 20 mm/s (printing speed). Before FDM 3D printing, the Gel-Lay filament was left in a laboratory oven at 65 °C for 1 h to remove potential moisture on it. After which, the filament was exported to the printing system for the initial 3D fabrication process. The printed Gel-Lay material was changed from rigid plastic to flexible elastomer after completely leaching out the rigid synthetic polymer, PVA, which plays as an add-on to enhance the printability of the filament for the FDM printing procedure.

To enhance cell viability in the BV construct, fibrin gel, a degradable biocompatible polymer formed from enzymatic crosslinking of fibrinogen and thrombin, was used as an inner layer material. After sequential steps to optimize the blending ratio of fibrinogen and thrombin to obtain the ideal viscosity for fibrin gel, 25 U/mL of thrombin solution was prepared by human plasma thrombin (100 U) diluting into PBS solution (4 mL). The fibrinogen solution with a concentration of 50 mg/mL was prepared by dissolving fibrinogen powders into 0.9% (w/v) NaCl solution. For inner layer printing, a custom-designed coaxial bioplotting system was used. The bioplotting system was equipped with needles (inner diameter: 1.2 mm and outer diameter: 1.6 mm) to extrude cell-laden fibrinogen (the inner needle) and thrombin (the outer needle) solutions at 1 mm/s (printing speed), 0.1 mL/s (extrusion flow rate), and room temperature (printing temperature) [10].

2.2. Optimization of 3D printing material

Gel-Lay disk (8 mm × 2 mm) (D × H) and strip (10 mm × 20 mm × 2 mm) (L × W × H) samples with three different infill densities, i.e., 100%, 70%, and 30%, were 3D printed at 215 °C with three different printing patterns including linear (LN), square (SQ), and hexagonal (HX). The time to eliminate PVA from the Gel-Lay material was investigated using the disk samples. The samples were completely submerged in a 48-well plate with de-ionized water (dH_2O) for up to 14 days, and the water was replaced every 6 h to maintain its freshness. The compressive moduli of the discs and tensile moduli of the strips were measured before and after leaching out the PVA components. Before each measurement, the samples were completely dried in an oven at 75 °C for 3 h. The mechanical properties of each sample were measured using an MTS Criterion universal testing system (MTS Systems Corp). To acquire the compressive modulus, the Gel-Lay discs were placed on the system equipped with a 10 kN load limit. The discs were compressed at a 1 mm/min strain rate until their breaking points. The compressive modulus of each sample was obtained from the linear elastic region slope of the stress-strain graph [36]. The measurement of tensile modulus was also performed. Briefly, the samples were vertically held by wedge grips and elongated at a strain rate of 1 mm/min until their breakpoints. Then, the tensile modulus of each strip was obtained in the same way as the compressive modulus. The mechanical properties of the 3D printed Gel-Lay BV scaffolds with 2 mm × 50 mm (D × L) was also characterized using the same protocol.

The surface topography of the 3D printed BV scaffolds before and after leaching out PVA was characterized by an FEI Teneo LV scanning electron microscope (SEM) (Thermo Fisher Scientific). The outer layers of the samples were coated with a 3 nm Au sheet and underwent a 5 kV potential difference from a 0.2 nA to 13 pA electron beam for image capturing [36].

Additionally, the weight change of the printed Gel-Lay BV scaffolds was quantified in phosphate-buffered saline (PBS) solution at 37 °C for up to 14 days during the PVA removal process. After each time point, i.e., 1, 7, 10, and 14 days, the samples were washed with fresh PBS solution and dried in an oven at 75 °C for 2 h before the measurement. The retention weight percentage of the scaffold was calculated based on the following equation [36].

$$\text{Retention wt } \% = 100 - \left\{ \left(\frac{w_r}{w_i} \right) \times 100 \right\} (\%)$$

where W_i and W_r are the measured initial and remaining weights of the samples.

2.3. Cell culture

hSMCs and HUVECs (Life Technologies) with single-digit passages were used in the preliminary cell viability studies. Cascade Biologics™ medium 231 with smooth muscle growth supplement (Gibco) and endothelial growth media (EGM) (Cell Applications) were applied as the culture medium for hSMCs and HUVECs, respectively.

Methods to obtain iSMC or iEC from iPSC can be classified into several approaches, including cell culture on extracellular matrix (ECM)/ gelatin coating (iSMC), or coculture with stromal cells (iEC) [30, 37–39]. Among them, the most common and mutual method for both cell types is to generate embryoid bodies (EBs), which utilizes the instinctive differentiation of iPSCs in a manner of a self-aggregated structure and their innate characteristic to resemble early embryonic development [30,38]. In our study, iSMCs and iECs were obtained from the Laboratory of Cardiovascular Regenerative Medicine at the National Institute of Health (NIH) (Bethesda, MD). All experiments were performed with iSMCs and iECs of single-digit passages. iSMCs were cultured in SmGM™−2 smooth muscle cell growth basal medium with SingleQuots™ supplements and growth factors (Lonza). iECs were cultured in a 1:1 ratio blended EBM™−2 endothelial cell growth basal medium with EGM™−2 endothelial SingleQuots™ kit (Lonza) and human endothelial SFM (Gibco). For passaging of the cells, TrypLE™ express trypsin (Gibco) was used. Also, a 1:1 total volume ratio of blended cell culture media was used to co-culture different cell lines.

2.4. Fabrication of iSMC (or hSMC) and iEC (or HUVEC)-laden inner layers

The printing process of the inner layer was discussed above (Section 2.1). For the cell encapsulation, isolated iSMCs (or hSMCs) were suspended in the fibrinogen solution to be simultaneously extruded in the FDM printed outermost layer at a 3000 cells/μL concentration under the extrusion conditions mentioned above, 1 mm/s (printing speed), 0.1 mL/s (extrusion flow rate), and room temperature (printing temperature). When the cell-laden fibrinogen and thrombin solutions came in contact at a 1:1 volumetric ratio via coaxial needle, an iSMC (or hSMC)-laden fibrin gel layer was formed. Similarly, the innermost fibrin gel layer with iECs (or HUVECs) at a 6000 cells/μL concentration was fabricated onto the iSMC (or hSMC) layer. The overall experimental procedure is schematically described in Fig.1.

2.5. Quantification and visualization of cell viability

In order to quantify cell proliferation rate, the seeded cells on each

specimen with a density of 500 cells/mm^2 were cultured in a 48-well plate at 37 °C with 5% CO_2 concentration for 7 days. The cell proliferation was quantified via a cell counting kit (CCK-8, Dojindo Molecular Technologies) after 1, 4, and 7 days. In detail, the cell counting solution (400 μL) that consists of 90% (v/v) cell culture medium and 10% (v/v) CCK-8 reagent was added to each well, and the entire well plates were left in an incubator for 3 h. Following that, the supernatant in each well (200 μL) was further added into a 96-well plate and the absorbance at 450 nm wavelength was measured via a Thermo Scientific Multiskan GO Spectrophotometer.

For visual observation of cell viability, a live-dead cell staining kit (BioVision) was utilized following the enclosed protocol. Cell viability of each cell line on the fabricated specimen with the same seeding density was observed using a Zeiss LSM 710 confocal microscope (Carl Zeiss AG) after 1, 4, and 7 days of culturing. Additionally, F-actin staining was performed to evaluate the cell spreading morphology after 1, 4, and 7 days. Before the staining process, the scaffolds were rinsed three times with PBS. Then, the cells were fixed and permeabilized for 15 mins using 10% formalin and 0.1% Triton X-100. After washing the scaffolds with PBS several times, the cells were stained with Texas red™-X phalloidin (Invitrogen) for 1 h and 4, 6-diamidino-2-phenylindole dihydrochloride (DAPI) (Invitrogen) for 15 mins, respectively [36].

To observe the distribution and growth of two different cell lines in the BVs, iSMCs, and iECs were pre-labeled by CellTracker™ Green CMFDA and CellTracker™ Orange CMTMR Dye (Thermo Fisher Scientific). Then, each cell line was suspended and blended with fibrin gel to form the two layers of BVs. The z-stack images of the BV construct were obtained using the confocal microscope after the same time intervals (1, 4, and 7 days). BVs with iECs and iSMCs were co-cultured in the mixed cell growth medium.

2.6. Immunofluorescence staining

To investigate the bioactivity of iSMCs and iECs in the fabricated BV, after 1 week of culture, the adhered cells were fixed and permeabilized for 15 mins. After washing with PBS three times, the scaffolds were incubated with a 1% (w/v) bovine serum albumin blocking solution for 1 h at 37 °C to block the unspecific binding antibodies. Once the blocking buffer was aspirated, the scaffolds were incubated overnight at 4 °C with α-SMA (ab7817) and CD31 (ab28364), which were used as the primary antibodies. On the next day, the scaffolds were rewashed with PBS and incubated with the secondary antibodies, Alexa Fluor™ 594 goat anti-mouse IgG H&L (Red, Thermo Fisher Scientific) and Alexa Fluor™ 488 goat anti-rabbit IgG H&L (Green, Thermo Fisher Scientific) for 1 h at 37 °C. The stained samples were imaged under the confocal microscope [17].

2.7. Statistical analysis

The quantitative data are presented as the mean ± standard deviation ($n = 9$). Data were analyzed by the one-way analysis of variance (ANOVA) with student's *t*-test to analyze statistically significant differences among groups. A p-value <0.05 was considered to be statistically significant [17,36].

3. Results and discussions

3.1. Optimization of outermost flexible BV material

The fundamental goal of this study was to obtain the vasculogenic potential of iPSCs in a flexible BV frame that satisfies physical and biomedical requirements. To investigate the effects of printing conditions on physical parameters first, a series of 3D printed Gel-Lay discs and strips with 100%, 70%, and 30% infill densities and LN, SQ, and HX printing patterns (total 9 groups) before and after PVA leaching out were optimized. These patterns and infill densities of 3D printing have been widely used as the basic elements in the fabrication of tissue constructs, including artificial BV fabrication. It was demonstrated that the weight change of each sample in the different groups started stabilizing after 7 days. As a result, there was no significant change between 7 and 14 days (varying 1.6% ± 0.9% weight change between 7 and 10 days and 0.86% ± 0.7% between 10 and 14 days) which could be attributed to the slow biodegradation of polyamide (the main component of Gel-Lay), compared to the 36.8% ± 5.4% weight loss between 1 and 7 days, regardless of printing pattern or infill density (Fig.2a). In other words, the complete removal of PVA from the Gel-Lay material could require around 7 days.

The physical tolerance against high blood pressure is an essential factor for artificial BV to survive in a dynamic flow condition. In the mechanical durability tests for material optimization, it was noticed that there were descending trends in both compressive and tensile moduli as infill density decreased within the same printing pattern group as expected. Also, the LN and SQ samples with 100% infill density possessed tensile and compressive rigidities each, compared to other groups (Fig.2b). Considering the contraction and relaxation nature of a BV, a tensile elongation, which is directly related to the stretchability of the printing material, is considered a more significant factor than the compressive modulus for a BV study. As a result, it was optimized that the use of the 100% LN group for the BV fabrication is advantageous in this perspective. It was also noticed that the surface roughness of the Gel-Lay materials changed after dissolving PVA in dH_2O. The removal of PVA resulted in a higher surface area in all 9 groups, regardless of the printing pattern and infill density as shown in SEM images (Supplementary Figs. 1–3), which is beneficial as a larger number of cells can be attached to the surface.

3.2. Characterization of optimized printed flexible small-diameter BV scaffolds

To further characterize the optimized outermost layer Gel-Lay BV scaffolds, the 100% LN group was printed to investigate their surface morphologies and mechanical properties using similar approaches above. The surface morphology of 3D printed BV with the dimension of (2 mm × 50 mm) (D × L) before and after PVA removal was characterized. As expected, it was observed that the BV sample prior to PVA removal possessed the minimum surface roughness with no obvious pattern. In contrast, the BV sample with the absence of PVA resulted in a higher surface area with a distinctive parallel alignment to the direction of 3D printing (Fig.3a–c). The obvious difference in stretchability between the two groups could be visually observed as shown in Fig.3d. Upon the completion of dissolving PVA in dH_2O, the elongation rate at the breakpoint of the BV sample significantly increased from 113.82% to 262.67%. In other words, the stretchability of the fabricated BV construct was enhanced more than 2.5 times compared to the original printed BV construct, which is higher than an electrospun polyurethane BV graft and its combination with other polymers, such as PCL [40]. Moreover, the permeability of the BV structure that plays a critical role in intercellular communication with its neighbor tissues and cells was visually reinforced after the PVA removal process (Fig.3e), demonstrating this structure could mimic complex fibrous constructs of ECM. Although many investigators attempted to obtain architectures that resemble native ECM, most of the previous studies utilized the native major components of ECM, such as collagen, elastin, gelatin, and glycosaminoglycan [41–45]. As an effective means of artificial vessel fabrication that uses synthetic polymers, the discovery of this strengthened flexibility and permeability is significant. Along with that, the tensile modulus of the BV sample after PVA removal was still rigid enough. It is known that BVs in the human body exhibit around 20–50 kPa and 100–200 kPa tensile moduli at the initial and post-radius expansion steps, respectively [46,47]. Although the absence of PVA resulted in a downturn of tensile modulus, that of the BV sample held similar durability to the native carotid artery in the human body

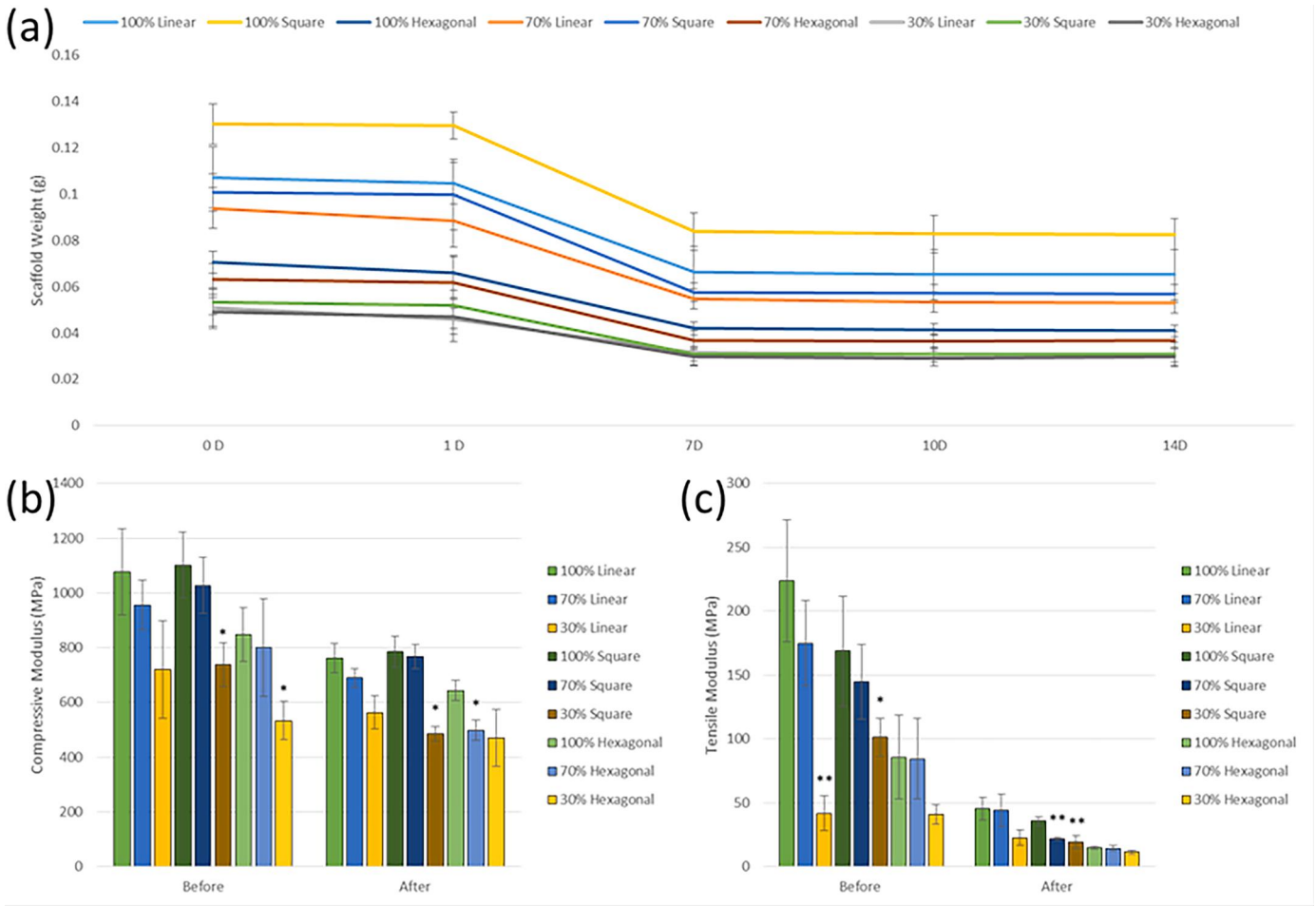

Fig. 2. (a) Weight change quantification of the 3D printed Gel-Lay samples with different infill densities (30%, 70%, and 100%) and printing patterns (LN, SQ, and HX) throughout the PVA removal process for 14 days. (b) Compressive moduli of the 3D printed Gel-Lay samples before and after PVA removal. (c) Tensile moduli of the 3D printed Gel-Lay samples before and after PVA removal. *: $p < 0.05$ and **: $p < 0.01$ when compared to 100% infill density groups of the same printing pattern. Data are the mean ± standard deviation; $n = 9$.

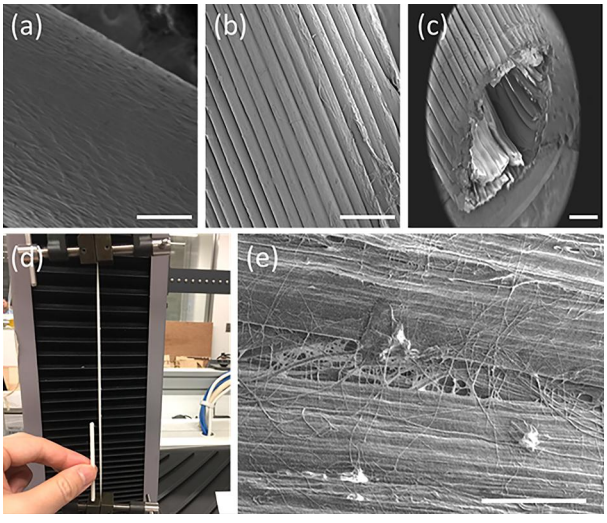

Fig. 3. SEM images of the 3D printed BV samples (a) before and (b) after PVA removal. The surface morphologies of the samples became remarkably different after PVA removal. Scale bars, 500 μm. (c) A cross-sectional SEM image of the 3D printed BV after PVA removal. Scale bar, 1 mm. (d) A photo image shows the enhanced stretchability of the 3D BV samples after PVA removal. (e) A magnified SEM image of the 3D printed BV sample after PVA removal, in which porous and fibrous structures can be observed. Scale bar, 100 μm.

Table 1
Comparison of tensile modulus and elongation at the breakpoint of the Gel-Lay BV construct before and after PVA removal with the native BV (carotid artery of men) [48].

	Tensile Modulus (MPa)	Elongation at Break (%)
Before PVA Removal	86.62	113.82
After PVA Removal	0.62	262.67
Native BV [48]	0.607	N/A

(Table 1) [48] and higher than previously reported 3D hydrogel based-BV graft studies [31,49]. It was important to demonstrate that the outermost supporting layer of an artificial BV possessed superior stretchability as well as sufficient tensile durability, which proves that our design can sustain in an environment with high blood pressure when transplanted into a patient at the level of *in vivo* and clinical demonstrations.

3.3. Evaluation of cellular behaviors in 3D printed BV construct

To confirm that the presence of the Gel-Lay material does not affect the viability of the laden cells within the fibrin gel layers of the printed BV constructs, a preliminary biocompatibility study using hSMCs and HUVECs were performed with other prevalent supporting materials for cell culture and tissue regeneration, including PCL, PLA, and gelatin methacrylate (GelMA) for comparison. As shown in Fig.4a, b, the cell

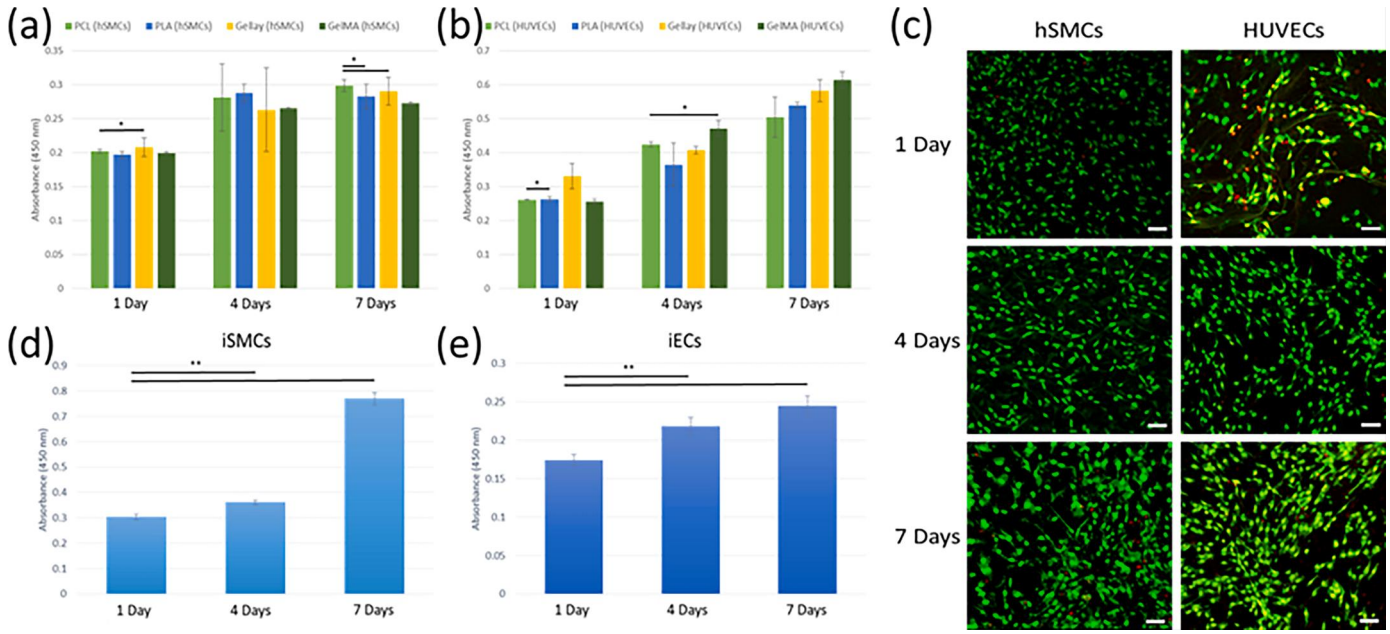

Fig. 4. Cell proliferation quantification of the (a) hSMCs and (b) HUVECs-laden fibrin gel layer in outer BV layers when using different biomaterials. (c) Confocal fluorescence microscope images of live/dead staining of hMSCs and HUVECs after 1, 4, and 7 days of culture in the 3D printed BV constructs. Scale bars, 100 μm. Cell proliferation quantification of (d) iSMCs and (e) iECs-laden fibrin gel layer in the Gel-Lay outer BV layer. *: $p < 0.05$ and **: $p < 0.01$. Data are the mean ± standard deviation; $n = 9$.

proliferation rate was not much affected by the types of the outer layer supporting materials due to the proper biocompatibility. In other words, the fibrin gel layers provided an optimal environment for cell growth, regardless of the outermost layer's biocompatibility. Furthermore, a series of live/dead staining tests were performed with hSMCs and HUVECs to investigate whether the engineered 3D constructs could be biocompatible with other BV cell lines. As a result, the 3D printed vessel structure could also be modeled with hSMCs and HUVECs (Fig.4c). Similarly, the cell proliferation rate was quantified for iSMCs and iECs, having Gel-Lay as an outer layer, and a similar pattern was demonstrated despite the innate slow proliferation of iECs (Fig.4d, e). Based on that, it was observed that the degree of biocompatibility of the outermost material was not a critical factor in our study due to the existence of the fibrin gel layers.

To visually explore the changes in cellular behavior, F-actin staining was performed for iSMCs and iECs within fiber gel of BV constructs separately after 7 days of culture. As shown in Fig. 5a–c, cell staining images of iSMCs demonstrated that the embedded cells appeared to be elongated and proliferated within the mid-fibrin gel layer. iECs, which have a smaller size than iSMCs, also demonstrated an increase in numbers being irregularly patterned from 1 to 7 days in the innermost fibrin layer (Fig. 5d–f). Additionally, the CellTracker™ stained images for both cell lines showed a similar tendency in terms of cell growth over 7 days of culturing. As shown in Fig. 6a–c, the growth and migration of iSMCs (red) and iECs (green) within their layer indicated successful vascularization and the formation of smooth muscle and endothelium. After 1 day, iSMCs were properly attached, elongated, and expanded in the fibrin gel layer due to their rapid proliferation and superior regenerative potential [31]. Approaching day 7, the development of both layers not only in the longitudinal but in the transversal direction was also observed, which is related to maturing myogenesis and vasculogenesis.

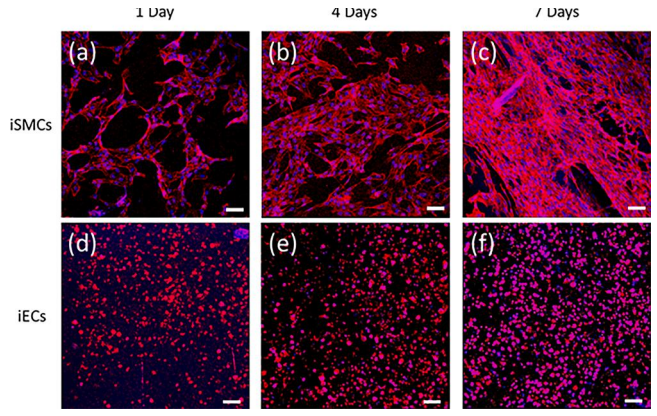

Fig. 5. Confocal microscope images of iSMCs (a–c) and iECs (d–f) after 1, 4, and 7 days in the 3D printed middle and innermost fibrin gel layers of our printed BV constructs. Scale bars, 100 μm.

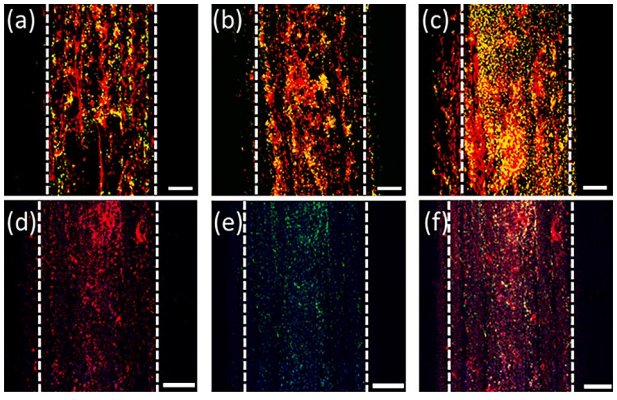

Fig. 6. Confocal microscope images of CellTracker™ stained iSMCs (red) and iECs (green) after (a) 1 day, (b) 4 days, and (c) 7 days of culture when coaxially extruded with a fibrinogen solution and a thrombin solution to form the fibrin gel layers. Scale bars, 500 μm. Confocal microscope immunofluorescence images of the 3D printed BV construct with (d) iSMCs, (e) iECs, and (f) both (merged), after 1 week of culture in the fibrin gel layers. α-SMA (red) and CD31 (green) primary antibodies with DAPI (blue) were used to identify iSMCs and iECs, respectively. Scale bars, 500 μm.

To further investigate the development of cell function, iSMCs and iECs were visually evaluated by the immunocytochemistry of the formed smooth muscle and endothelium in the 3D printed BV with iSMCs and iEC-specific biomarkers, such as α-SMA and CD31 primary antibodies after 1 week of cell culture. As shown in Fig.6d–f, it was demonstrated that the engagement of the biomarkers to both cell lines was enhanced, despite the relatively slower-growing nature of iECs. These results imply that the cells laden in the fibrin layers can successfully lead to the development of a mature endothelium as well as a smooth muscle to mimic the natural BV structure.

Generally, our approach using iPSCs can be significantly beneficial since the proliferation and differentiation abilities of human stem cells substantially decrease as donors age [30], which prevents acquiring sufficient numbers of autologous cells for damaged BV reconstruction. Hence, the successfully established fabrication protocol for the formation of smooth muscle and endothelium in the 3D BV constructs with patient-specific iSMCs and iECs can significantly contribute to the advancement of BV-related disease treatment. Although we have successfully developed 3D flexible BV grafts *in vitro* using a unique combination of multiple 3D printing techniques, the printer resolution is still limited to create BVs at a smaller scale. The development of high-resolution bioprinting systems or advanced nanobioinks will help us manufacture novel BVs at varied scales.

4. Conclusion

As vascularization is the most important process for the repair of damaged BV that is caused by associated diseases, the successful fabrication of artificial BV can significantly contribute to the essential vasculogenesis of ECs and myogenesis of vascular SMCs, which will result in an adequate integration with the surrounding tissues. The integration of mechanical and biological aspects accounts for a critical role in acquiring an optimal BV fabrication process; however, it has yet to be achieved. In the present study, we exhibited that the incorporation of a flexible rubber-like elastomer and a fibrin gel with embedded iSMCs and iECs using FDM 3D printing and coaxial bioplotting technologies could successfully generate excellent small-diameter BV constructs with similar morphology to native BVs. The use of our FDM printed rubber-like Gel-Lay elastomer as an outermost layer would provide essential support until the 3D printed BV is remodeled by the host environment in the human body. Additionally, the iSMCs and iECs-laden fibrin gel layers formed from fibrinogen and thrombin were printed by the coaxial bioplotting as two inner layers to compensate for the lack of bioactivity of the Gel-Lay layer and to improve the BV regeneration. Based on their durability and perfusability, the BVs could withstand blood pressure and support nutrient transport, which hold great potential for future clinical vessel replacement and vascularized tissue regeneration. Moreover, there are several future study directions to further validate our BV design: (1) a dynamic culture condition replicating the physiologically relevant microcirculation system to obtain a confluent iEC layer and to test vascular contractile functions, and (2) an *in vivo* study to demonstrate its performance for clinical applications.

Declaration of Competing Interest

The authors declare that there are no conflicts of interest.

Data Availability

Data will be made available on request.

Acknowledgment

The authors would like to thank the financial support from NSF Biomechanics and Mechanobiology Program Award Number 1854415 and American Heart Association Transformative Project Award. We also thank the George Washington University Center for Microscopy and Image Analysis.

Supplementary materials

Supplementary material associated with this article can be found, in the online version, at doi:10.1016/j.bea.2022.100065.

References

[1] S.Y. Hann, H. Cui, T. Esworthy, S. Miao, X. Zhou, S.J. Lee, et al., Recent advances in 3D printing: vascular network for tissue and organ regeneration, Transl. Res. J. Lab. Clin. Med. (2019).
[2] H. Cui, M. Nowicki, J.P. Fisher, L.G. Zhang, 3D bioprinting for organ regeneration, Adv. Healthc. Mater. 6 (2017).
[3] H. Cui, S. Miao, T. Esworthy, X. Zhou, S.J. Lee, C. Liu, et al., 3D bioprinting for cardiovascular regeneration and pharmacology, Adv. Drug Deliv. Rev. (2018).
[4] S.S. Virani, A. Alonso, H.J. Aparicio, E.J. Benjamin, M.S. Bittencourt, C. W. Callaway, et al., Heart disease and stroke statistics—2021 update: a report from the American Heart Association, Circulation 143 (2021) e254–e743.
[5] C.K. Zarins, D.P. Giddens, B. Bharadvaj, V.S. Sottiurai, R.F. Mabon, S. Glagov, Carotid bifurcation atherosclerosis. Quantitative correlation of plaque localization with flow velocity profiles and wall shear stress, Circ. Res. 53 (1983) 502–514.
[6] J.G. Nemeno-Guanzon, S. Lee, J.R. Berg, Y.H. Jo, J.E. Yeo, B.M. Nam, et al., Trends in tissue engineering for blood vessels, J. Biomed. Biotechnol. (2012), 2012.
[7] T.L.B. Ha, T.M. Quan, D.N. Vu, Naturally derived biomaterials: preparation and application. Regenerative Medicine and Tissue Engineering, IntechOpen, 2013.
[8] C. Dikyol, M. Altunbek, B. Koc, Embedded multimaterial bioprinting platform for biofabrication of biomimetic vascular structures, J. Mater. Res. (2021) 1–14.
[9] Y. Gu, C. Tian, Y. Qin, Y. Sun, S. Liu, H. Li, et al., The novel hybrid polycarbonate polyurethane/polyester three-layered large-diameter artificial blood vessel, J. Biomater. Appl. (2021), 08853282211033415.
[10] X. Zhou, M. Nowicki, H. Sun, S.Y. Hann, H. Cui, T. Esworthy, et al., 3D bioprinting-tunable small-diameter blood vessels with biomimetic biphasic cell layers, ACS Appl. Mater. Interfaces 12 (2020) 45904–45915.
[11] L.G. Griffith, B. Wu, M.J. Cima, M.J. Powers, B. Chaignaud, J.P. Vacanti, *In vitro* organogenesis of liver tissuea, Ann. N. Y. Acad. Sci. 831 (1997) 382–397.
[12] N.N. Zein, I.A. Hanouneh, P.D. Bishop, M. Samaan, B. Eghtesad, C. Quintini, et al., Three-dimensional print of a liver for preoperative planning in living donor liver transplantation, Liver Transpl. 19 (2013) 1304–1310.
[13] S. Pashneh-Tala, S. MacNeil, F. Claeyssens, The tissue-engineered vascular graft—Past, present, and future, Tissue Eng. B Rev. 22 (2016) 68–100.
[14] V.V. Alvino, A.C. Thomas, M.T. Ghorbel, F. Rapetto, S.A. Narayan, M. Kilcooley, et al., Reconstruction of the swine pulmonary artery using a graft engineered with syngeneic cardiac pericytes, Front. Bioeng. Biotechnol. (2021) 806.
[15] N. Yudintceva, Y.A. Nashchekina, M. Shevtsov, V. Karpovich, G. Popov, I. Samusenko, et al., Small-diameter vessels reconstruction using cell tissue-engineering graft based on the polycaprolactone, Cell Tissue Biol. 15 (2021) 577–585.
[16] J.A. Beckman, Diseases of the Veins, Circulation 106 (2002) 2170–2172.
[17] S.Y. Hann, H. Cui, N.C. Zalud, T. Esworthy, K. Bulusu, Y.L. Shen, et al., An *in vitro* analysis of the effect of geometry-induced flows on endothelial cell behavior in 3D printed small-diameter blood vessels, Biomater. Adv. (2022), 212832.
[18] S.Y. Hann, H. Cui, M. Nowicki, L.G. Zhang, 4D printing soft robotics for biomedical applications, Addit. Manuf. (2020), 101567.
[19] K.K. Sankaran, K.S. Vasanthan, U.M. Krishnan, S. Sethuraman, Development and evaluation of axially aligned nanofibres for blood vessel tissue engineering, J. Tissue Eng. Regen Med. 8 (2014) 640–651.
[20] G. Pitarresi, C. Fiorica, F.S. Palumbo, S. Rigogliuso, G. Ghersi, G. Giammona, Heparin functionalized polyaspartamide/polyester scaffold for potential blood vessel regeneration, J. Biomed. Mater. Res. A 102 (2014) 1334–1341.
[21] A.J. Guerra, P. Cano, M. Rabionet, T. Puig, J. Ciurana, 3D-printed PCL/PLA composite stents: towards a new solution to cardiovascular problems, Materials 11 (2018) 1679 (Basel).
[22] D. Pfeiffer, C. Stefanitsch, K. Wankhammer, M. Müller, L. Dreyer, B. Krolitzki, et al., Endothelialization of electrospun polycaprolactone (PCL) small caliber vascular grafts spun from different polymer blends, J. Biomed. Mater. Res. A 102 (2014) 4500–4509.
[23] T. Agarwal, G.M. Fortunato, S.Y. Hann, B. Ayan, K.Y. Vajanthri, D. Presutti, et al., Recent advances in bioprinting technologies for engineering cardiac tissue, Mater. Sci. Eng. C Mater. Biol. Appl. 124 (2021), 112057.
[24] H. Altinova, S. Hammes, M. Palm, P. Achenbach, J. Gerardo-Nava, R. Deumens, et al., Dense fibroadhesive scarring and poor blood vessel-maturation hamper the integration of implanted collagen scaffolds in an experimental model of spinal cord injury, Biomed. Mater. 15 (2020), 015012.
[25] H. Stratesteffen, M. Köpf, F. Kreimendahl, A. Blaeser, S. Jockenhoevel, H. Fischer, GelMA-collagen blends enable drop-on-demand 3D printablility and promote angiogenesis, Biofabrication 9 (2017), 045002.
[26] A. Lee, A. Hudson, D. Shiwarski, J. Tashman, T. Hinton, S. Yerneni, et al., 3D bioprinting of collagen to rebuild components of the human heart, Science 365 (2019) 482–487.
[27] X. Cui, T. Boland, Human microvasculature fabrication using thermal inkjet printing technology, Biomaterials 30 (2009) 6221–6227.

[28] S. Yamanaka, A fresh look at iPS cells, Cell 137 (2009) 13–17.
[29] H. Inoue, N. Nagata, H. Kurokawa, S. Yamanaka, iPS cells: a game changer for future medicine, EMBO J. 33 (2014) 409–417.
[30] Y. Wang, J. Hu, J. Jiao, Z. Liu, Z. Zhou, C. Zhao, et al., Engineering vascular tissue with functional smooth muscle cells derived from human iPS cells and nanofibrous scaffolds, Biomaterials 35 (2014) 8960–8969.
[31] B.C. Dash, K. Levi, J. Schwan, J. Luo, O. Bartulos, H. Wu, et al., Tissue-engineered vascular rings from human iPSC-derived smooth muscle cells, Stem Cell Rep. 7 (2016) 19–28.
[32] Y. Lin, C.H. Gil, M.C. Yoder, Differentiation, evaluation, and application of human induced pluripotent stem cell–derived endothelial cells, Arterioscler. Thromb. Vasc. Biol. 37 (2017) 2014–2025.
[33] C.K. Su, J.Y. Lin, 3D-printed column with porous monolithic packing for online solid-phase extraction of multiple trace metals in environmental water samples, Anal. Chem. 92 (2020) 9640–9648.
[34] F. Li, N.P. Macdonald, R.M. Guijt, M.C. Breadmore, Multimaterial 3D printed fluidic device for measuring pharmaceuticals in biological fluids, Anal. Chem. 91 (2019) 1758–1763.
[35] J. You, R.J. Preen, L. Bull, J. Greenman, I. Ieropoulos, 3D printed components of microbial fuel cells: towards monolithic microbial fuel cell fabrication using additive layer manufacturing, Sustain. Energy Technol. Assess. 19 (2017) 94–101.
[36] S.Y. Hann, H. Cui, T. Esworthy, X. Zhou, S.J. Lee, M.W. Plesniak, et al., Dual 3D printing for vascularized bone tissue regeneration, Acta Biomater. 123 (2021) 263–274.
[37] B.C. Dash, Z. Jiang, C. Suh, Y. Qyang, Induced pluripotent stem cell-derived vascular smooth muscle cells: methods and application, Biochem. J. 465 (2015) 185–194.
[38] Y. Lin, C.H. Gil, M.C. Yoder, Differentiation, evaluation, and application of human induced pluripotent stem cell-derived endothelial cells, Arterioscler. Thromb. Vasc. Biol. 37 (2017) 2014–2025.
[39] M.C. Yoder, Differentiation of pluripotent stem cells into endothelial cells, Curr. Opin. Hematol. 22 (2015) 252–257.
[40] A. Abdal-Hay, M. Bartnikowski, S. Hamlet, S Ivanovski, Electrospun biphasic tubular scaffold with enhanced mechanical properties for vascular tissue engineering, Mater. Sci. Eng. C 82 (2018) 10–18.
[41] S. Heydarkhan-Hagvall, K. Schenke-Layland, A.P. Dhanasopon, F. Rofail, H. Smith, B.M. Wu, et al., Three-dimensional electrospun ECM-based hybrid scaffolds for cardiovascular tissue engineering, Biomaterials 29 (2008) 2907–2914.
[42] I. Jun, H.S. Han, J.R. Edwards, H. Jeon, Electrospun fibrous scaffolds for tissue engineering: viewpoints on architecture and fabrication, Int. J. Mol. Sci. 19 (2018) 745.
[43] K. Thomas, A.J. Engler, G.A. Meyer, Extracellular matrix regulation in the muscle satellite cell niche, Connect. Tissue Res. 56 (2015) 1–8.
[44] S.L. Wen, S. Feng, S.H. Tang, J.H. Gao, L.H. Zhang, H. Tong, et al., Collapsed reticular network and its possible mechanism during the initiation and/or progression of hepatic fibrosis, Sci. Rep. 6 (2016) 1–11.
[45] J.K. Mouw, G. Ou, V.M. Weaver, Extracellular matrix assembly: a multiscale deconstruction, Nat. Rev. Mol. Cell Biol. 15 (2014) 771–785.
[46] D. Wang, Y. Xu, Q. Li, L.S. Turng, Artificial small-diameter blood vessels: materials, fabrication, surface modification, mechanical properties, and bioactive functionalities, J. Mater. Chem. B 8 (2020) 1801–1822.
[47] C.J. Van Andel, P.V. Pistecky, C. Borst, Mechanical properties of porcine and human arteries: implications for coronary anastomotic connectors, Ann. Thorac. Surg. 76 (2003) 58–64.
[48] A.V. Piterina, A.J. Cloonan, C.L. Meaney, L.M. Davis, A. Callanan, M.T. Walsh, et al., ECM-based materials in cardiovascular applications: inherent healing potential and augmentation of native regenerative processes, Int. J. Mol. Sci. 10 (2009) 4375–4417.
[49] L. Xu, M. Varkey, A. Jorgensen, J. Ju, Q. Jin, J.H. Park, et al., Bioprinting small diameter blood vessel constructs with an endothelial and smooth muscle cell bilayer in a single step, Biofabrication 12 (2020), 045012.